

# TAMM: Tensor Algebra for Many-body Methods

Erdal Mutlu,<sup>1, a)</sup> Ajay Panyala,<sup>1, b)</sup> Nitin Gawande,<sup>2</sup> Abhishek Bagusetty,<sup>3</sup> Jeffrey Glabe,<sup>1</sup> Jinsung Kim,<sup>4</sup> Karol Kowalski,<sup>5</sup> Nicholas P. Bauman,<sup>5</sup> Bo Peng,<sup>5</sup> Himadri Pathak,<sup>1</sup> Jiri Brabec,<sup>6</sup> and Sriram Krishnamoorthy<sup>7, c)</sup>

<sup>1)</sup>*Advanced Computing, Mathematics, and Data Division, Pacific Northwest National Laboratory, Richland, Washington 99354, United States*

<sup>2)</sup>*Intel Corporation, Portland, Oregon, United States*

<sup>3)</sup>*Argonne Leadership Computing Facility, Argonne National Laboratory, Argonne, Illinois 60439, United States*

<sup>4)</sup>*School of Computer Science and Engineering, Chung-Ang University, Seoul 06974, South Korea*

<sup>5)</sup>*Physical Sciences Division, Pacific Northwest National Laboratory, Richland, Washington 99354, United States*

<sup>6)</sup>*J. Heyrovský Institute of Physical Chemistry, Academy of Sciences of the Czech Republic, 182 23 Prague 8, Czech Republic*

<sup>7)</sup>*Google Inc., Mountain View, California 94043, United States*

Tensor contraction operations in computational chemistry consume a significant fraction of the computing time on large-scale computing platforms. The widespread use of tensor contractions between large multi-dimensional tensors in describing electronic structure theory has motivated the development of multiple tensor algebra frameworks targeting heterogeneous computing platforms. In this paper, we present Tensor Algebra for Many-body Methods (TAMM)<sup>1</sup>, a framework for productive and performance-portable development of scalable computational chemistry methods. TAMM decouples the specification of the computation and the execution of these operations on available high-performance computing systems. With this design choice, the scientific application developers (domain scientists) can focus on the algorithmic requirements using the tensor algebra interface provided by TAMM, whereas high-performance computing developers can direct their attention to various optimizations on the underlying constructs, such as efficient data distribution, optimized scheduling algorithms, and efficient use of intra-node resources (e.g., GPUs). The modular structure of TAMM allows it to support different hardware architectures and incorporate new algorithmic advances. We describe the TAMM framework and our approach to the sustainable development of tensor contraction-based methods in computational chemistry applications. We present case studies highlighting the ease of use, including the performance and productivity gains compared to other implementations.

## I. INTRODUCTION

Enabling highly-scalable computational environments that abstract and automate the coding of complex numerical operations is critically needed to advance computational chemistry towards more complex and accurate formulations capable of taking advantage of emerging exascale computing architectures and as a foundation for sustainability and portability of the software for chemistry. In particular, tensor contractions (TCs) are a universal language used in many areas of quantum mechanics to encode equations describing collective phenomena in many-body quantum systems encountered in quantum field theory, quantum hydrodynamics, nuclear structure theory, material sciences, and quantum chemistry. Typically, contractions between multi-dimensional tensors stem from the discretization procedures to represent the Schrödinger equation in a finite-dimensional algebraic form. An important area where tensor contractions play a crucial role is electronic structure theory, where tensors describe basic interactions and parameters defining wave function expansions.

One of the most critical applications of TCs is the coupled-cluster (CC) formalism.<sup>2-9</sup> In the CC theory, the form of the

complex TCs used to represent non-linear equations describing the correlated behavior of electrons in molecular systems also reflects on the fundamental feature of the CC formalism referred to as the size-extensivity or proper scaling of the energy with the number of particles. For this reason, CC formalism is one of the most accurate computational models used these days in computational chemistry.

The CC theory has assumed a central role in high-accuracy computational chemistry and still attracts much attention in theoretical developments and numerical implementations. In this effort, high-performance computing and the possibility of performing TCs in parallel play an essential role in addressing steep polynomial scaling as a function of system size and extending CC formalism to realistic chemical problems described by thousands of basis set functions. To understand the scale of the problem, the canonical CC formulations such as the ubiquitous CCSD(T) approach<sup>10</sup> (CC with the iterative single and double excitations with non-iterative corrections due to triple excitations) involve contractions between four-dimensional tensors where ranges of thousands of entries can define each dimension. In order to alleviate efficient CC calculations on parallel platforms, several specialized tensor libraries have been developed over the last decade.

In the last few decades, significant effort has been expended toward enabling CC simulations for very large chemical systems to extend the applicability of the CC formalism further. In the reduced-scaling formulations, commonly referred to as the local CC methods,<sup>11-19</sup> one takes advantage of the local

<sup>a)</sup>Electronic mail: [erdal.mutlu@pnnl.gov](mailto:erdal.mutlu@pnnl.gov)

<sup>b)</sup>Electronic mail: [ajay.panyala@pnnl.gov](mailto:ajay.panyala@pnnl.gov)

<sup>c)</sup>Electronic mail: [sriram.krishnamoorthy@gmail.com](mailto:sriram.krishnamoorthy@gmail.com)

character of correlation effects to effectively reduce the number of parameters and the overall cost of CC iterations. Using even small computational clusters, the (DLPNO-CC)<sup>15-19</sup> formalism can be performed for systems described by 10,000-40,000 basis set functions. The limit for the system size can be further extended by utilizing parallel exascale architectures. However, to achieve this goal, several computational challenges associated with the data representation, distribution, and optimization of the DLPNO-CC equations (characterized by a large number of contractions and tensors involved in the underlying equations) have to be appropriately addressed. This paper discusses a new tensor library, Tensor Algebra for Many-body Methods (TAMM), which provides a flexible environment for expressing and implementing TCs for canonical and local CC approximations. The development of TAMM functionalities for the ground-state formulations (canonical CCSD and CCSD(T) methods and local CC formulations) was supported by the NWChemEx project<sup>20</sup>, whereas excited-state formulations (CC Green's function, Equation-of-Motion CC, and real-time CC) by the SPEC project<sup>21</sup>.

As high-performance computing systems evolve to include different types of accelerators, diverse memory hierarchy configurations, and varying intra- and inter-node topologies, there is a need to enable the decoupling of the development of CC methods and their optimization for various platforms. TAMM enables the compact specification of various tensor-contraction methods while allowing independent yet incremental development of optimization strategies to map these methods to current and emerging computing platforms.

In the rest of the paper, we introduce the TAMM framework that allows the efficient implementation of various CC methods on high-performance computing systems. Section II gives detailed information about previous and current tensor algebra frameworks that is used in scientific applications. Later in Section III, we describe the details of our tensor algebra interface and underlying constructs that are used to efficiently distribute tensor data and execute tensor operations on new high-performance computing systems. Section IV showcases multiple CC methods implemented with TAMM frameworks and new performance results collected on large-scale runs on the Summit Supercomputer. Finally, Section V concludes our paper introducing the TAMM framework.

## II. REVIEW OF EXISTING INFRASTRUCTURE

Tensor-based scientific applications have been widely used in different domains, from scientific simulation to more recent machine learning-based scientific applications. Over the years, program synthesis and code generation have become the go-to solution for such applications. The Tensor Contraction Engine (TCE),<sup>22</sup> which is used in the NWChem computational chemistry software package<sup>23</sup>, has been the most successful state-of-the-art solution for generating parallel code for various molecular orbital (MO) basis CC methods in Fortran 77. In later work, the TCE project<sup>24</sup> added support for optimizations on tensor expression factorization, optimized code generation for various hardware, and space-time trade-offs for helping to

implement more complex electronic structure methods, mainly for CC methods.

In a separate effort, the FLAME project<sup>25</sup> provided formal description support for describing linear algebra operations over matrices with support of the optimized implementation of these kernels for distributed memory systems. Later, various studies over-optimizing tensor algebra<sup>26-28</sup> have been proposed using the FLAME framework.

More recently, the Cyclops Tensor Framework (CTF)<sup>29</sup> was developed, aiming at more efficient kernel implementation for tensor operations using concurrency. The framework focused on reducing the required communication in parallel executions of CC-based methods by using a triangular dense tensor representation. Epifanovsky *et al.*<sup>30</sup> developed an object-oriented C++ library called `libtensor` for efficient execution of post-Hartree-Fock electronic structure methods using a blocked representation of large size dense tensors. In a later work<sup>31</sup>, they optimized various operations by efficient memory management techniques that is thread-friendly and NUMA-aware. Both frameworks focus on dense tensors and do not account for the block sparsity within the computation.

Solomonik and Hoefler extended CTF for general sparse computations.<sup>32</sup> Manzer *et al.* demonstrated the benefits of exploiting block sparsity in electronic structure theory calculations.<sup>33</sup> Neither approach includes notational support for the general block-structured nature of the sparsity that naturally occurs in electronic structure methods.

Orca is a general quantum chemistry program involving implementations of reduced-scaling methods. In order to achieve the speed up, various approximations are employed, for example, density fitting, RIJ-COSX, or local approach for NEVPT2 or CC methods. The C++ code employs MPI-based parallelization schemes, and recently, in a pilot study, they implemented a scheme for generating 3- and 4-index integrals via accelerators.<sup>34</sup>

The TiledArray framework<sup>35</sup> is actively being developed for scalable tensor operations supporting different computational chemistry methods<sup>36</sup>. It makes use of the Multi Resolution Adaptive Numerical Environment for Scientific Simulation (MADNESS) parallel runtime framework<sup>37</sup> that employs a high-level software environment for increasing both programmer productivity and code scalability in massively parallel systems. TiledArray employs a hierarchical view of sparsity coupled with explicit user-written loop nests to perform specialized sparse operations over sparse tensors.

Finally, ExaTensor<sup>38</sup> library uses a domain-specific virtual processors concept for allowing performance portable programming and execution of tensor operations on modern GPU systems (i.e., NVidia, AMD etc.). While the library is mostly focused on general GPU computation and the portability of such operations to different systems, they demonstrated the effectiveness on a numerical tensor algebra workloads that mainly focusses the quantum many-body computations in large scale GPU accelerated HPC platforms.

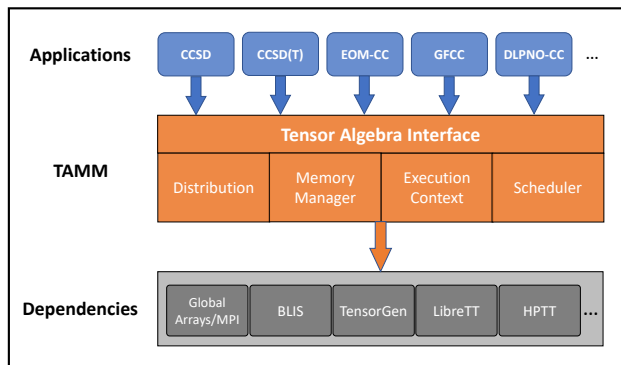


Figure 1: Overview of Tensor Algebra for Many-body Methods (TAMM) Framework

### III. TAMM FRAMEWORK

This section will give a detailed explanation of our tensor algebra framework. Figure 1 shows the conceptual overview of our framework. TAMM provides a tensor algebra interface that allows users to describe tensor operations in a familiar mathematical (Einstein) notation while underneath it employs efficient data distribution/management schemes as well as efficient operation execution on both CPU-based and GPU-based hardware. Our framework leverages efficient libraries such as HPTT<sup>39</sup> for efficient tensor index permutations on CPUs, LibreTT<sup>40</sup> for efficient tensor index permutations on GPUs and Global Arrays<sup>41</sup>, a partitioned global address space (PGAS) programming model for efficient data distribution. The role of these libraries is discussed in more detail in the following subsections.

#### A. Tensor Algebra Operations in TAMM

TAMM provides a flexible infrastructure for describing tensor objects using the general notion of an *index space* (simply an index range) that is used to describe the size of each dimension. TAMM also employs tiling capabilities where users can define arbitrary or fixed size tiling over *index spaces* to construct *tilted index spaces* to represent a blocked representation of a tensor. This allows tensors to be constructed as a set of smaller blocks of data indexed by the Cartesian product of the number of tiles on each dimension. This notion of tiling enables efficient data distribution and efficient tensor operations (i.e., tensor contractions) that can better leverage the underlying hardware by utilizing the available cache system as well as the execution modules (i.e., GPUs, CPUs, etc.). TAMM’s flexible tiling capabilities provide crucial support for load balancing and making effective trade-offs over data communication and efficient computation. These optimizations will be detailed in the next subsection, where we describe the data communication and execution of tensor operations.

Figure 2 shows an example of *index space*, *tilted index space*, and *tensor* construction in the TAMM framework. Lines 2–4 show the construction of `IndexSpace`

```

1 // Constructing index spaces
2 IndexSpace N{range(100)};
3 IndexSpace M{range(30)};
4 IndexSpace K{range(20)},
5     {"first", {range(0, 10)}},
6     {"second", {range(10, 20)}}
7     };
8
9 // Tiling the index spaces
10 TiledIndexSpace tN{N, 10};
11 TiledIndexSpace tM{M, {10,20}};
12 TiledIndexSpace tK{K, 5};
13
14 // Constructing a tensor object
15 Tensor <double> A{tM, tK};
16 Tensor <double> B{tK, tN};
17 Tensor <double> C{tM, tN};

```

Figure 2: Source code example for `IndexSpace`, `TiledIndexSpace`, and `Tensor` construction using TAMM.

objects that represent a range of indices using a range constructor. Our framework also allows users to describe application-specific annotations over the subsections of these spaces. Lines 4–7 show an example of string-based annotation over subsections of the construction range. This allows users to easily access different portions of an index space, thereby enabling access to slices of a tensor and constructing new tensors using slices of the original index space. Similarly, users can encode *spin* information related to each dimension over the input tensors allowing our run-time to allocate these tensors using a block-sparse representation. For the time being, we only support spin symmetry for representing the block sparsity. Users can define their own non-zero check functionality to be used on allocation and tensor operation execution for both space and computational benefits. Additional capabilities, such as restricted summations or point group and permutational symmetries, are not supported in the tensor specification. Point group symmetry is less concerning since TAMM targets large systems that often do not have such symmetry. However, developers can explicitly code these features using TAMM to construct the desired tensors. This is the case for methods such as CCSD(T), discussed in Section IV A 2.

Lines 10–12 show the construction of `TiledIndexSpace` objects that represent a sliced index space that is used in tensor construction to have a blocked structure. Tiling can be applied as a fixed size (i.e., line 10) or as arbitrary tile sizes with full coverage of the index space (i.e., line 11). Finally, lines 15–17 in Figure 2 show the construction of `Tensor` objects using tiled index spaces. Each `TiledIndexSpace` object used in the tensor constructor represents a dimension in constructed tensors. In this example, tensor `A` is a  $30 \times 20$  matrix with eight blocks as denoted by `tM` which consists of two tiles of sizes 10 and 20 while `tK` consists of four tiles that are size 5. While these lines construct a tensor object, the tensor is collectively allocated by all participating compute nodes in a subsequent operation

---

```

1 // construct tN labels
2 auto [a, b, c] = tN.labels<3>();
3 // construct tM labels
4 auto [i, j, k] = tM.labels<3>();
5 // construct tK labels
6 auto [l, m, n] = tK.labels<3>();
7 // construct subspaces of tK
8 auto [x, y, z] = tK("first").labels<3>();

```

---

Figure 3: Source code example for constructing index labels.

using a *scheduler*.

Another important concept in constructing tensor operations is *index labels* that allows to specify the tensor operation similar to Einstein notation and provide slicing capabilities over tensors by using the string-based subsections of the full index space. Labels are associated with *tiled index spaces* and used in the tensor operation syntax to describe the computation. Depending on the index spaces that the tensors are constructed on, users can specify string-based sub-spaces to define operations on different slices of the underlying allocated tensor object. Figure 3 shows examples of `TiledIndexLabel` construction using `TiledIndexSpace` objects. While lines 1-6 construct the labels over the full spaces, line 8 shows the label creation for the *first* portion of `tK` index space (see construction on Figure 2 line 4). These sub-spaces can then be used for specifying operations over sliced portions of the full tensor as long as the index labels are from a subset of the original index space.

$$\begin{aligned}
\langle \text{tensor-op} \rangle &::= \langle \text{op-lhs} \rangle = \langle \text{op-rhs} \rangle & (1) \\
&| \langle \text{op-lhs} \rangle += \langle \text{op-rhs} \rangle & (2) \\
&| \langle \text{op-lhs} \rangle -= \langle \text{op-rhs} \rangle & (3) \\
\langle \text{op-lhs} \rangle &::= \langle \text{label-tensor} \rangle & (4) \\
\langle \text{op-rhs} \rangle &::= \langle \text{alpha} \rangle & (5) \\
&| \langle \text{label-tensor} \rangle & (6) \\
&| \langle \text{alpha} \rangle * \langle \text{label-tensor} \rangle & (7) \\
&| \langle \text{alpha} \rangle * \langle \text{label-tensor} \rangle * \langle \text{label-tensor} \rangle & (8) \\
\langle \text{label-tensor} \rangle &::= \langle \text{tensor-id} \rangle ( \langle \text{label-list} \rangle ) & (9) \\
\langle \text{alpha} \rangle &::= \text{tensor value type} & (10)
\end{aligned}$$

Figure 4: Tensor operations grammar in extended Backus–Naur form.

TAMM supports three main tensor operations: tensor set, tensor addition, and tensor contraction. Figure 4 gives the grammar for allowed tensor operations’ syntax in the TAMM framework. Each tensor operation syntax rule ( $\langle \text{tensor-op} \rangle$ ) is composed of a left-hand side (lhs,  $\langle \text{op-lhs} \rangle$ ) and a right-hand side (rhs,  $\langle \text{op-rhs} \rangle$ ) operation. While *lhs* can only be a labeled tensor construct ( $\langle \text{label-tensor} \rangle$ ), *rhs* can be of different types that result in a different tensor operation:

- alpha value ( $A(i, l) = \text{alpha}$ ), which corresponds

to a tensor set operation that assigns the corresponding alpha value to all elements of the tensor.

- labeled tensors ( $A(i, l) += \text{alpha} * D(l, i)$ ) correspond to a tensor addition operation (with respect to the label permutation on tensor D) in Eq. (6).
- contraction of two labeled tensors ( $C(i, a) += \text{alpha} * A(i, l) * B(l, a)$ ) updates the lhs with the tensor contraction results in Eq. (7).

Similar to tensor allocation, all other tensor operations that use and modify the distributed tensor data have to be performed via a *scheduler* that has necessary information about the *execution context* from the operation. *Execution context* includes required information about the distribution scheme of the tensor data and the execution medium for the operations through *distribution*, *memory manager*, and *process group* constructs. TAMM employs a modular construction of these concepts to allow users to implement various distribution schemes as well as use of different distributed memory frameworks. Figure 5 shows the construction of a `Scheduler` object using the *execution context* and execution of defined tensor operations. After creating a scheduler, users can directly queue the tensor operations such as tensor allocation (line 12), tensor set and add operations (lines 13-14), and tensor contractions (line 15). Finally, all queued operations are executed using the *execution context* on a distributed system. The tensor operations, as well as the operations over the index spaces, are formally described in our previous work<sup>42</sup>. The syntax for expressing operations shown in lines 13-15 also indicates the productivity benefits that can be obtained by using TAMM. The operations expressed in these three lines are executed in parallel on CPUs or GPUs or both on any distributed computing platform. Manually writing parallel code for these operations would lead to a significant increase in the source lines of code (SLOC). Extending such manual development of parallel code to a real application with a large number of such operations would only lead to a significant increase (orders of magnitude) in the SLOC count and development time which would also make future improvements to such code infeasible.

This section summarized the tensor algebra interface as an embedded domain-specific language (eDSL) into the TAMM framework. By implementing an eDSL, we were able to have separation of concerns for developing scientific applications. While the high-level tensor abstractions allowed domain scientists to implement their algorithms using a representation close to mathematical formulation, it also allowed framework developers to test various different optimization schemes on the underlying constructs (i.e., different data distribution schemes, operation execution on accelerators, use of different PGAS systems etc.) which we will detail in the coming section.

## B. Tensor Distribution and Operation Execution in TAMM

TAMM leverages various state-of-the-art frameworks and libraries to achieve a scalable performance-portable implemen-

---

```

1 // Constructing process group, memory manager, distribution
2 // to construct an execution context
3 ProcGroup pg = ProcGroup::create_coll (GA_MPI_Comm());
4 auto manager = MemoryManagerGA::create_coll(pg);
5 auto distribution = DenseDistributio
6 ExecutionContext ec{pg, & distribution , manager};
7
8 // Constructing a scheduler for executing tensor operations
9 Scheduler sch{&ec};
10
11 // Tensor operations are queued for execution into the Scheduler
12 sch. allocate (A, B, C)
13 (A(i, 1) = 1.0) // SetOp – Grammar rule (5)
14 (B(i, 1) = A(i, 1)) // AddOp – Grammar rule (6)
15 (B(i, 1) += -1.0 * A(i, 1)) // AddOp – Grammar rule (7)
16 (C(i, a) = 0.5 * A(i, 1) * B(i, a)) // MultOp – Grammar rule (8)
17 // All queued operations are executed.
18 .execute ();

```

---

Figure 5: Source code example for executing the tensor operations using TAMM.

tation of tensor algebra operations on exascale supercomputing platforms through efficient data distribution and intra-node execution of tensor operation kernels on CPUs and GPUs. The default *memory manager* for tensor data distribution in TAMM is based on the Global Arrays framework, a Partitioned Global Address Space (PGAS) programming model that provides a shared memory-like programming model on distributed memory platforms. Global Arrays provides performance, scalability, and user productivity in TAMM by managing the inter-node memory and communication for tensors. A TAMM tensor is essentially a global array with a certain distribution scheme. We have implemented three tensor distribution schemes in TAMM. The first scheme computes an effective processor grid for a given number of MPI ranks. A dense tensor is then mapped onto the processor grid. The second scheme is a simple round-robin distribution that allocates equal-sized blocks in a round-robin fashion where the block size is determined by the size of the largest block in the tensor. This distribution over-allocates memory and ignores sparsity. The third scheme allocates the tensor blocks in a round-robin fashion while taking block sparsity into account. By only allocating non-zero blocks in the tensor, it minimizes the memory footprint of overall computation, allowing bigger-sized problems to be mapped to the available resources.

TAMM uses the “Single Program Multiple Data (SPMD)” model for distributed computation. In this programming abstraction, each node has its own portion of tensors available locally as well as access to the remote portions via communication over the network. As a result, operations on the whole tensors can result in access to remote portions on the tensor, with implied communication. More importantly, many operations (i.e., tensor contractions, addition, etc.) are implied to be collective as they involve the distributed tensors as a whole. While the tensor algebra interface follows a sequential ordering of tensor operations, we also tried to conceal the burden of thinking in a distributed manner while writing a scientific application. To avoid possible issues with operations on distributed

tensors, TAMM is designed to represent tensors in terms of handles and requires tensor operations to be declared explicitly and executed using a *scheduler*. Hence, any assignment done on tensor objects will be a shallow copy as opposed to a deep copy, as a deep copy implies communication (message passing between nodes to perform the copy operation).

The computational chemistry methods are implemented as a sequence of operations over distributed tensors. Through this design, we were able to separate the specification of the operations from their implementations, allowing method developers to mainly focus on the computational chemistry algorithms while kernel developers can focus on the optimization of individual tensor operations. Execution of all tensor operations is managed by a scheduler. The TAMM scheduler employs a data flow analysis over the queued tensor operations to find the dependencies between each operation in order to load balance the computation and communication requirements of the overall execution. Using a leveled execution scheme, the scheduler is able to limit the global synchronizations to achieve load-balanced and communication-efficient schedules for the execution of all tensor operations. The dependency analysis over the high-level operations is based on a macro operation-graph. When two or more operations share the same tensor object and one of these operations updates the shared object, the operations are marked as conflicting operations that can not be executed in parallel. This operation-graph is used to construct a batch of operations that can be executed in parallel, minimizing the total number of global synchronizations required by the computation. The operations in these batches are then executed in an SPMD fashion. For instance, canonical CCSD implementation in TAMM has 10 levels of operation batches that sum to over 125 tensor operations.

While TAMM hides the burden of choosing the best-performing schedule from the users through load-balanced scheduler execution, it allows users to control various aspects of the computation, such as data distribution, parallelization strategies, operation ordering, and execution medium (i.e., CPUs, GPUs). To achieve this, TAMM uses a modular structure to describe constraints imposed by the users to automate the construction of an execution plan for efficient execution of the computation. This allows users to incrementally optimize their code with minimal programming effort while keeping it readable as opposed to a code generator-based solution. With these controls over the execution and distribution of the tensor data, users can choose from different optimizations at different granularity. For example, the user can increase the data locality by replicating frequently used small tensors on each distributed node or choosing from different distribution schemes for efficient tensor operation execution on various node topologies. Such an optimization can be implemented as a new data distribution scheme (i.e., SUMMA<sup>43</sup>) by extending the `Distribution` class. By simply using this distribution, users can enforce a specific distribution on tensors which can optimize required data communication for specific operations. Another abstraction for optimization is on the actual computation of the tensor operations. Users can define new operations by extending the `Op` class which can then be scheduled to be executed. While TAMM supports the most common operations

defined on tensors (i.e., addition, contraction), it also implements a `Scan` and `Map` operation that can be used to define various element/block-wise operations using lambda functions. Additionally, as a lower-level abstraction, users also can decide to describe new executions specific for a new architecture/accelerator on the kernel level (i.e., DGEMM, GPU abstraction). While TAMM supports main GPUs (i.e., NVidia, AMD, Intel) that will be available in upcoming HPC systems, users can also choose to implement new kernel-level abstractions for different hardware stacks (i.e., FPGAs, ML/DL accelerators).

To achieve highly optimized execution of tensor operations on a given platform, TAMM is designed to allow use of multiple external libraries that provides optimized kernels for various operations. In addition to leveraging vendor-provided linear algebra libraries that are highly tuned for both CPUs and GPUs, TAMM also uses the following libraries: HPTT<sup>39</sup> library for optimized tensor index permutations on CPUs, LibreTT<sup>40</sup> for enabling efficient index permutation on NVIDIA, AMD and Intel GPUs, BLIS<sup>44</sup> library for efficient BLAS implementation in CPU and lastly, TensorGen<sup>45</sup> for generating optimized tensor contraction GPU kernels specialized for CC methods in computational chemistry.

While TAMM tries to hide the execution details from the end-user by employing high-level tensor algebra expressions, users can specify the medium on which they want the operations to be executed. Users can specify a particular operation to be executed on CPU or GPU. All other execution-specific details like parallelization, CPU to GPU communication, and execution mechanisms are handled automatically by TAMM infrastructure. While TAMM does not explicitly rely on OpenMP, it can leverage OpenMP for important operations like tensor transposition and GEMM via highly optimized external libraries such as HPTT and vendor BLAS. Setting the `OMP_NUM_THREADS` variable before running any TAMM-based application would enable OpenMP parallelization.

In this section, we have provided a detailed explanation of the optimizations and dependencies we employ in our framework. TAMM leverages a modular infrastructure to enable the implementation of various optimizations on different levels of the computation, from data distribution to execution schemes on different hardware. This design allowed us to implement different *memory managers*, *distribution* schemes, and work distribution over different *process groups* without any major changes to the user-facing tensor algebra interface. The following section describes the impact of using TAMM for implementing various coupled cluster methods arising in computational chemistry.

#### IV. CC TAMM IMPLEMENTATIONS

In this section, we present case studies where TAMM is used to implement various coupled-cluster (CC) methods for the latest HPC systems. While important, TAMM’s primary contributions are not the faster methods but the ability to productively develop and explore new algorithms, and apply those improvements to all existing and new methods implemented using TAMM. This includes improvements in intra-node ex-

ecution (single core, OpenMP multicore, GPUs, etc.), data distribution strategies (e.g., replication, process group-based distribution), and parallel execution (compute partitioning and communication scheduling algorithms). It also allows the concurrent development of optimized equations, parallel algorithms, and optimized intra-node kernels by different teams through clearly defined interfaces. The variety of methods presented and their performance is evidence that this approach accelerates the development and exploration of CC methods.

#### A. Canonical Methods

The canonical formulations of the Coupled-Cluster (CC) formalisms<sup>2-7,9</sup> are based on the exponential parametrization of the correlated ground-state wave function  $|\Psi\rangle$ :

$$|\Psi\rangle = e^T |\Phi\rangle, \quad (11)$$

where  $T$  is the cluster operator and the so-called reference function  $|\Phi\rangle$  in single-reference formulations is assumed to be represented by a Hartree–Fock Slater determinant. In practical realizations, it is assumed that  $|\Phi\rangle$  provides a good approximation to the correlated  $|\Psi\rangle$  state. The cluster operator  $T$  can be partitioned into it many body components  $T_k$

$$T = \sum_{k=1}^N T_k, \quad (12)$$

defined as

$$T_k = \frac{1}{(k!)^2} \sum_{i_1, \dots, i_k; a_1, \dots, a_k} t_{a_1 \dots a_k}^{i_1 \dots i_k} a_{a_1}^\dagger \dots a_{a_k}^\dagger a_{i_k} \dots a_{i_1}, \quad (13)$$

where  $a_p^\dagger$  ( $a_p$ ) are the creation (annihilation) operators for an electron in  $p$ -th state and indices  $i_1, i_2, \dots$  ( $a_1, a_2, \dots$ ) refer to occupied (unoccupied) spin orbitals in the reference function  $|\Phi\rangle$ . The operators  $T_k$ , defined by the cluster amplitudes  $t_{a_1 \dots a_k}^{i_1 \dots i_k}$ , produce  $k$ -tuple excitations when acting onto the reference function.

To define equations needed for determining cluster amplitudes, we introduce wave-function expansion (11) into the Schrödinger equation and pre-multiplying both sides by  $e^{-T}$ . This procedure leads to an explicitly connected form of the energy-independent equations for amplitudes and energy, i.e.,

$$\langle \Phi_{i_1 \dots i_k}^{a_1 \dots a_k} | e^{-T} H e^T | \Phi \rangle = 0, \forall k, \forall i_1, \dots, i_k, \forall a_1, \dots, a_k, \quad (14)$$

$$E = \langle \Phi | e^{-T} H e^T | \Phi \rangle, \quad (15)$$

where the electronic Hamiltonian  $H$  is defined as

$$H = \sum_{pq} h_q^p a_q^\dagger a_p + \frac{1}{4} \sum_{p,q,r,s} v_{rs}^{pq} a_r^\dagger a_s^\dagger a_q a_p \quad (16)$$

where  $h_q^p$  and  $v_{rs}^{pq}$  are tensors representing interactions in the quantum system and excited Slater determinants  $|\Phi_{i_1 \dots i_k}^{a_1 \dots a_k}\rangle$  are defined as

$$|\Phi_{i_1 \dots i_k}^{a_1 \dots a_k}\rangle = E_{i_1 \dots i_k}^{a_1 \dots a_k} |\Phi\rangle. \quad (17)$$

In all CC formulations discussed here, to form equations (14) for cluster amplitudes, one needs to (1) find an efficient way for distributing and compressing tensors  $h_q^p$ ,  $v_{rs}^{pq}$ ,  $t_{a_1 \dots a_k}^{i_1 \dots i_k}$  across all nodes, (2) define efficient algorithms for partitioning TCs of multi-dimensional tensors across the parallel system, and (3) optimize communication between nodes to minimize the effect of the latency. To illustrate the scale of the problems, in brute force simulations, we have to store 4-dimensional tensors  $t_{a_1 a_2}^{i_1 i_2}$  and  $v_{rs}^{pq}$  that require storage proportional to  $n_o^2 n_u^2$  and  $(n_o + n_u)^4$ , respectively, where  $n_o$  and  $n_u$  refer to the number of occupied and unoccupied orbitals in the reference function  $|\Phi\rangle$ . For CC simulations of the molecular systems defined by  $n_o = 200$  and  $n_u = 2,800$  one needs to distribute data of the order of 150 TB. Therefore, to make these simulations possible, the support from sophisticated HPC algorithms and applied math is indispensable.

### 1. Coupled Cluster Singles Doubles (CCSD)

The CCSD formalism (CC with single and double excitations)<sup>5</sup> is one of the most popular CC approximations and is used in routine computational chemistry calculations as a necessary intermediate step towards more accurate CC models, such as perturbative CCSD(T) formalism discussed in the next section, or excited-state or linear-response CC extensions. In the CCSD formalism, the cluster operator  $T$  is approximated as

$$T \simeq T_1 + T_2, \quad (18)$$

and the equations for cluster amplitudes are represented as

$$r_i^a = \langle \Phi_i^a | e^{-(T_1+T_2)} H e^{T_1+T_2} | \Phi \rangle, \quad (19)$$

$$r_{ij}^{ab} = \langle \Phi_{ij}^{ab} | e^{-(T_1+T_2)} H e^{T_1+T_2} | \Phi \rangle, \quad (20)$$

where the tensors  $r_i^a$  and  $r_{ij}^{ab}$  are commonly referred to as the residual vectors. Due to a large number of terms corresponding to complicated contractions between  $h_q^p/v_{rs}^{pq}$  and  $t_a^i/t_{ab}^{ij}$ , optimization of the expressions plays a crucial role. This is achieved by proper factorization by introducing the so-called recursive intermediates. For example,

$$\frac{1}{4} v_{mn}^{ef} t_{ef}^{ij} t_{ab}^{mn} \quad (21)$$

term, which contributes to  $r_{ij}^{ab}$  in the naive approach is characterized by  $n_o^4 n_u^4$  numerical overhead. However, by introducing the intermediate tensor  $I_{mn}^{ij}$  defined as (we assumed Einstein summation convention over repeated indices)

$$I_{mn}^{ij} = v_{mn}^{ef} t_{ef}^{ij}, \quad (22)$$

the term (21) can be given by the equation

$$\frac{1}{4} I_{mn}^{ij} t_{ab}^{mn} \quad (23)$$

at the total numerical cost proportional to  $n_o^4 n_u^2$ . Another important technique that is useful in reducing the memory footprint

of the CCSD approach is the Cholesky decomposition (CD) of the  $v_{rs}^{pq}$  tensor, i.e.,

$$v_{rs}^{pq} \simeq (pr|L)(L|qs) - (ps|L)(L|qr), \quad (24)$$

where  $L$  is an auxiliary index. The total memory required to store Cholesky vectors  $(pq|L)$  needed to reproduce  $v_{rs}^{pq}$  with high accuracy is usually proportional to  $(n_o + n_u)^3$ .

As benchmark systems for testing the performance of TAMM implementations of the Cholesky-based CCSD<sup>46</sup>, we used two molecular systems previously used in studying the efficiency of the TCE implementations of the CC methods in NWChem<sup>47,48</sup>. The first benchmark system is the model of Bacteriochlorophyll (BChl)  $\text{MgC}_{36}\text{N}_4\text{O}_6\text{H}_{38}$ ,<sup>49,50</sup> which plays an important role in understanding the mechanism of photosynthesis. In this process, the light is harvested by antenna systems and further funneled to BChl molecules that initiates primary charge separation. The second benchmark system considered here is the  $\beta$ -carotene molecule, whose doubly excited states and triplet electronic states have recently been intensively studied in the context of singlet fission processes in carotenoid aggregates<sup>51-53</sup>. The  $\beta$ -carotene molecule consists of 96 atoms, while the BChl model contains 85 atoms, including a central magnesium atom. We use the cc-pVDZ basis for both systems and evaluate the performance on OLCF Summit<sup>54</sup>. Each Summit node contains two IBM POWER9 processors, each consisting of 22 cores, and 512GB of CPU memory. Each node is also equipped with 6 NVIDIA Volta GPUs, each with 16GB memory, leading to a total of 96GB GPU memory per node.

Table I shows the CCSD performance compared to NWChem on 200 nodes of OLCF Summit. We measure the performance of the TAMM implementations against the TCE implementations in NWChem. Time per CCSD iteration is given in seconds. NWChem has CPU-only implementation and uses 42 CPU cores on each node of Summit. TAMM-based Cholesky-CCSD uses only 6 MPI ranks per node, where each MPI rank is mapped to a single GPU. For these two molecular systems, we observe a 9-15 $\times$  speedup with the TAMM-based Cholesky-CCSD implementation compared to the TCE CCSD method in NWChem. The CPU implementation of the CCSD tensor operations in NWChem comprises 11,314 source lines of code whereas the Cholesky-CCSD implementation expressed using the TAMM framework is only 236 source lines of code. Since these 236 lines represent the computation at a high level, they express both CPU and GPU computation. On the other hand, adding GPU capabilities to the NWChem CCSD code will only significantly increase the SLOC count and development time which is why a GPU implementation for CCSD was not attempted to this date in NWChem. This clearly demonstrates the productivity benefits of expressing such computations in TAMM. Our implementation of the CCSD equations<sup>46</sup> are expressed similar to as shown in the example in Figure 5. CCSD is an example of how TAMM can be used to productively create an effective and efficient implementation of certain classes of computational chemistry methods. The remaining computational chemistry methods discussed in this paper are also implemented along similar lines.

Table I: TAMM performance compared to NWChem on 200 nodes of OLCF Summit. Time per CCSD iteration is given.

Molecule	#Atoms	# Occupied Orbitals	#Basis Functions	Time (s)	
				NWChem <sup>55</sup>	TAMM
BChl	85	171	852	1202	81
$\beta$ -carotene	96	148	840	801	65

## 2. Coupled Cluster Triples

The CCSD(T) formalism<sup>10,56</sup> is capable in many cases of providing the so-called chemical level of accuracy required in studies of chemical reactivity and thermochemistry. In the CCSD(T) approach the perturbative correction due to triple excitations ( $E^{(T)}$ ) is added to the CCSD energy:

$$E^{\text{CCSD(T)}} = E^{\text{CCSD}} + E^{(T)}, \quad (25)$$

where

$$E^{(T)} = \sum_{\substack{i < j < k \\ a < b < c}} \frac{\langle \Phi | (T_2^+ V_N) | \Phi_{ijk}^{abc} \rangle \langle \Phi_{ijk}^{abc} | V_N T_2 | \Phi \rangle}{\varepsilon_i + \varepsilon_j + \varepsilon_k - \varepsilon_a - \varepsilon_b - \varepsilon_c} + \sum_{\substack{i < j < k \\ a < b < c}} \frac{\langle \Phi | T_1^+ V_N | \Phi_{ijk}^{abc} \rangle \langle \Phi_{ijk}^{abc} | V_N T_2 | \Phi \rangle}{\varepsilon_i + \varepsilon_j + \varepsilon_k - \varepsilon_a - \varepsilon_b - \varepsilon_c}, \quad (26)$$

where  $V_N$  is the two-body part of the electronic Hamiltonian in a normal product form, and  $|\Phi_{ijk}^{abc}\rangle = a_a^\dagger a_b^\dagger a_c^\dagger a_k a_j a_i |\Phi\rangle$ . The most expensive part of the CCSD(T) calculation, characterized by the  $n_o^4 n_u^3 + n_o^3 n_u^4$  scaling, is associated with calculating the  $\langle \Phi_{ijk}^{abc} | V_N T_2 | \Phi \rangle$  term, which is defined as

$$\begin{aligned} \langle \Phi_{ijk}^{abc} | V_N T_2 | \Phi \rangle = & v_{ma}^{ij} t_{bc}^{mk} - v_{mb}^{ij} t_{ac}^{mk} + v_{mc}^{ij} t_{ab}^{mk} - v_{ma}^{ik} t_{bc}^{mj} + v_{mb}^{ik} t_{ac}^{mj} + \\ & v_{mc}^{ik} t_{ab}^{mj} + v_{ma}^{jk} t_{bc}^{mi} - v_{mb}^{jk} t_{ac}^{mi} + v_{mc}^{jk} t_{ab}^{mi} - v_{ab}^{ei} t_{jk}^{ec} + \\ & v_{ac}^{ei} t_{jk}^{ec} - v_{bc}^{ej} t_{ia}^{ek} + v_{ab}^{ej} t_{ic}^{ek} - v_{ac}^{ej} t_{ib}^{ek} + v_{bc}^{ej} t_{ia}^{ek} - \\ & v_{ab}^{ek} t_{ij}^{ec} + v_{ac}^{ek} t_{ij}^{ec} - v_{bc}^{ek} t_{ij}^{ec}, \quad (i < j < k, a < b < c). \quad (27) \end{aligned}$$

Eq. (27) can be separated into terms  $A_{ijk}^{abc}$  and  $B_{ijk}^{abc}$ , defined by contractions over occupied indices ( $A_{ijk}^{abc}$ ; first nine terms on the right hand side (r.h.s.) of Eq. (27)) and terms corresponding to contraction over unoccupied indices ( $B_{ijk}^{abc}$ ; remaining nine terms on the r.h.s. of Eq. (27)), i.e.,

$$\langle \Phi_{ijk}^{abc} | V_N T_2 | \Phi \rangle = A_{ijk}^{abc} + B_{ijk}^{abc}. \quad (28)$$

Analogously, the  $\langle \Phi_{ijk}^{abc} | V_N T_1 | \Phi \rangle$  term takes the form

$$\begin{aligned} \langle \Phi_{ijk}^{abc} | V_N T_1 | \Phi \rangle = & v_{ab}^{ij} t_c^k - v_{ac}^{ij} t_b^k + v_{bc}^{ij} t_a^k \\ & - v_{ab}^{ik} t_c^j + v_{ac}^{ik} t_b^j - v_{bc}^{ik} t_a^j \\ & + v_{ab}^{jk} t_c^i - v_{ac}^{jk} t_b^i + v_{bc}^{jk} t_a^i \\ & (i < j < k, a < b < c). \quad (29) \end{aligned}$$

While Eqs. (27) and (29) can be easily implemented with the tensor operations mentioned in earlier sections, the performance of the (T) correction, in terms of both speed and memory, is improved by encoding key symmetries by hand while still using the distributed tensor data structure provided by TAMM. This includes the restricted index summation and permutational symmetries, which are not routine features in the current version of TAMM. In addition, the contractions in (T) are all fused so that the resulting output is a scalar instead of a 6-dimensional intermediate tensor. Currently, TAMM does not support fusion across contractions writing to the same output tensor, but this capability is considered for the near future. Furthermore, the hand-coded kernels for (T) for various GPU architectures are required for the best performance. In addition to fusion, we are also considering incorporating optimized GPU kernels in TAMM for specific contractions such as the ones in (T). The scheduler can then detect such contractions and choose the corresponding optimized kernels for execution rather than executing the contractions through the current default pipeline.

Table II shows the TAMM-based triples correction (T) calculation<sup>46</sup> performance compared to NWChem on 512 nodes of OLCF Summit. Time is given in seconds. NWChem has a GPU implementation of the triples correction and uses all 6 GPUs and 42 CPU cores on each node. The TAMM-based triples correction uses only 6 MPI ranks per node, where each MPI rank is mapped to a single GPU. For the BChl and  $\beta$ -carotene molecules, we observe a speedup of  $\sim 6$ - $18\times$  for the TAMM implementation compared to the TCE implementation in NWChem. The finer details of the TAMM-based triples correction implementation are detailed in Ref. 57.

Table II: TAMM performance compared to NWChem for the perturbative correction in the CCSD(T) method on 512 nodes of OLCF Summit.

Molecule	#Atoms	# Occupied Orbitals	#Basis Functions	Time (s)	
				NWChem <sup>55</sup>	TAMM
BChl	85	171	852	18285	1791
$\beta$ -carotene	96	148	840	6646	1164

## B. New Methods

### 1. Equation-of-Motion Coupled Cluster Formalism

The equation-of-motion (EOM) methods<sup>58-62</sup> and closely related linear response (LR) CC formulations<sup>63-65</sup> can be viewed as excited-state extensions of the single-reference CC theory. In the exact EOMCC formalism, the wave function for the K-th excited state  $|\Psi_K\rangle$  is represented as

$$|\Psi_K\rangle = R_K e^T |\Phi\rangle, \quad (30)$$

where  $R_K$  is the excitation operator, which produces the K-th excited state when acting onto the correlated ground-state



in CC representations. The energy of the  $K$ -th state and the amplitudes defining  $R_K$  operator can be calculated by solving non-Hermitian eigenvalue problem

$$\bar{H}R_K|\Phi\rangle = E_K R_K|\Phi\rangle, \quad (31)$$

where the similarity transformed Hamiltonian  $\bar{H}$  is defined as

$$\bar{H} = e^{-T} H e^T, \quad (32)$$

In the rudimentary EOMCCSD approximation (EOMCC with singles and doubles), the  $R_K$  and  $T$  operators are approximated as

$$R_K \simeq R_{K,0} + R_{K,1} + R_{K,2}, \quad (33)$$

$$T \simeq T_1 + T_2. \quad (34)$$

and the corresponding similarity transformed Hamiltonians is diagonalized in space defined by the reference function (for states non-orthogonal by symmetry to the reference function) and singly and doubly excited Slater determinants of required symmetry. The numerical scaling of the EOMCCSD approach, in analogy to the CCSD method, is dominated by  $n_o^2 n_u^4$  terms. The EOMCCSD method is usually employed in studies of excited states dominated by single excitations. It is also worth mentioning that LR-CC methods with singles and doubles leads to the same values of excited-state energies. However, in contrast to the EOMCCSD formalism, the LR-CCSD excitations are identified with the poles of frequency-dependent linear-response CC amplitudes.

Table III shows the TAMM EOMCCSD calculation performance compared to NWChem on 200 nodes of OLCF Summit. Time per EOMCCSD iteration is given in seconds. NWChem has CPU-only implementation and uses 42 CPU cores on each of the 200 nodes of Summit. Just as with the previous calculations, the TAMM-based EOMCCSD uses 6 MPI ranks per node, where each MPI rank is mapped to a single GPU. The current TAMM implementation of the EOMCCSD approach has not been optimized at the equation level as the CD-CCSD implementation. For example, in contrast to the CD-CCSD formalism, the EOMCCSD implementation fully represents 2-electron integrals and uses a non-spin-explicit representation of the operators in the equations. While we plan to return to this implementation and incorporate the optimized (spin-explicit) equations, we already observe a significant speed-up over NWChem with this primitive implementation. CD-CCSD and EOMCCSD calculations are different algorithms for solving the corresponding problem, and the timing for an iteration of EOMCCSD is a sum of all of the steps in an interaction, which tends to be more computationally demanding than the Jacobi step in CD-CCSD. Nonetheless, one can see from Table III that the TAMM EOMCCSD code is 2-3 times faster for  $\beta$ -carotene and BChl molecules.

## 2. Coupled Cluster Green's Function

The correlated formulations of Green's function methods are indispensable elements of the computational infrastructure

Table III: TAMM performance compared to NWChem on 200 nodes of OLCF Summit. Time per EOMCCSD iteration is given.

Molecule	#Atoms	# Occupied Orbitals	#Basis Functions	Time (s)	
				NWChem <sup>55</sup>	TAMM
BChl	85	171	852	2030	715
$\beta$ -carotene	96	148	840	1170	540

needed not only to calculate ionization potentials, electron affinities, and excitation energies but also as quantum solvers for various embedding formulations. The CC formalism provides a natural platform for the development of the one-body Green's function and the introduction of high-rank correlation effects.<sup>66-69</sup> Without loss of generality, here we will focus only on the retarded part of the Green's function (the advanced part can be developed in an analogous way) defined by matrix elements  $G_{pq}^R(\omega)$ :

$$G_{pq}^R(\omega) = \langle \Psi_g | a_q^\dagger (\omega + (H - E_0) - i\eta)^{-1} a_p | \Psi_g \rangle, \quad (35)$$

where  $E_0$  is the corresponding ground-state energy for  $N$ -electron system,  $\eta$  is a broadening factor, and  $|\Psi_g\rangle$  represents ground-state of  $N$ -electron system. In CC we are using different parametrizations for the bra ( $\langle \Psi_g |$ ) and ket ( $|\Psi_g\rangle$ ) wave functions,<sup>60,70</sup> i.e.,

$$\langle \Psi_g | = \langle \Phi | (1 + \Lambda) e^{-T} \quad (36)$$

$$|\Psi_g\rangle = e^T |\Phi\rangle, \quad (37)$$

which leads to the following form of retarded part of the CC Green's function (CCGF)<sup>66-69,71,72</sup>

$$G_{pq}^R(\omega) = \langle \Phi | (1 + \Lambda) \bar{a}_q^\dagger (\omega + \bar{H}_N - i\eta)^{-1} \bar{a}_p | \Phi \rangle. \quad (38)$$

The similarity transformed operators here  $\bar{A}$  ( $A = H, a_p, a_q^\dagger$ ) are defined as  $\bar{A} = e^{-T} A e^T$  (the  $\bar{H}_N$  stands for a normal product form of  $\bar{H}$ ). The numerically feasible algorithms for calculating (38) employ  $\omega$ -dependent auxiliary operators  $X_p(\omega)$

$$\begin{aligned} X_p(\omega) &= X_{p,1}(\omega) + X_{p,2}(\omega) + \dots \\ &= \sum_i x^i(\omega)_p a_i + \sum_{i<j,a} x_a^{ij}(\omega)_p a_a^\dagger a_j a_i + \dots, \quad \forall_p \end{aligned} \quad (39)$$

that satisfy equations

$$(\omega + \bar{H}_N - i\eta) X_p(\omega) | \Phi \rangle = \bar{a}_p | \Phi \rangle. \quad (40)$$

Using these operators matrix elements can be expressed in a simple form

$$G_{pq}^R(\omega) = \langle \Phi_g | (1 + \Lambda) \bar{a}_q^\dagger X_p(\omega) | \Phi_g \rangle. \quad (41)$$

In our implementation of CCGF formalism we approximate  $\Lambda$  operator by  $T^\dagger$ . The main numerical effort associated with the constructing retarded CC Green's function is associated with the need of solving a large number of independent linear equations, which in turn can contribute to efficient parallel schemes utilizing multiple levels of parallelism. Using TAMM,

we implemented CCGF at the singles and doubles level<sup>73</sup>. Reference 74 describes the CCGF implementation using TAMM in detail and also has a detailed analysis on its performance on OLCF Summit. We employed the same fundamental features of TAMM in the implementation of CCGF similar to our CCSD implementation and observe excellent performance and scalability. Our current implementation is publicly available<sup>73</sup>.

### C. DLPNO CCSD(T)

The development of reduced-scaling quantum chemical methods became a significant part of the recent research effort. In particular, for coupled cluster approaches, the local domain-based methods have been introduced and successfully applied on large systems.<sup>17,75</sup> Our implementation is inspired by the work cited as Ref. 17. The basic idea is to carefully take advantage of the local character of correlations effects. The total CCSD energy can be seen as a sum of  $ij$ -pair specific contributions  $\epsilon_{ij}$ :

$$E^{\text{CCSD}} = \sum_{ij} \epsilon_{ij}. \quad (42)$$

In order to significantly reduce the scaling, we are considering following tasks:

1. Differentiate pairs with respect to their energy contributions  $\epsilon_{ij}$  by sequential pre-screenings. Identify  $ij$ -pairs which a) are negligible and immediately dropped, b) can be evaluated at a lower-level model (MP2 level), and c) the pairs that can be evaluated at CC level.
2. Find an optimal representation of the virtual space for each  $ij$ -pair, in which the derived tensors (amplitudes, residuals, or integrals) are dense.
3. Find optimal factorization of terms in amplitude equations.
4. Perform only those tensor contractions which lead to non-zero results (including integral transformation and amplitude equations evaluation).

In the local pair natural orbital CCSD method, the occupied orbitals are localized (for example, by Pipek–Mezey or Foster–Boys algorithm<sup>76,77</sup>) and the virtual space is constructed specifically for a given occupied orbital pair. First, the virtual orbitals are transformed to a local basis of projected atomic orbitals (PAO)  $|\tilde{\mu}\rangle$  as  $|\tilde{\mu}\rangle = (1 - \sum_i |i\rangle\langle i|)\mu\rangle$ ,<sup>78–80</sup> which are a priori local and can be easily used to form domains corresponding to local occupied orbitals. In the next step pair natural orbitals (PNO) are constructed.<sup>16,17,81–84</sup> Thus, in Eqs. 19 and 20, instead of virtual index  $a, b, \dots$  we will get pair-specific PNOs  $\tilde{a}_{ij}, \tilde{b}_{ij}, \dots$  where we assume that the size of PNO space  $N(\text{PNO}(ij)) \ll N(\text{MO}_{\text{virt}})$ . The PNO spaces are obtained from pair density matrices  $\mathbf{D}^{ij}$

$$\mathbf{D}^{ij} = \tilde{\mathbf{T}}^{ij} \mathbf{T}^{ij\dagger} + \tilde{\mathbf{T}}^{ij\dagger} \mathbf{T}^{ij}, \quad (43)$$

where  $\mathbf{T}^{ij}$  are MP2 amplitudes in PAO basis

$$T_{\mu\nu}^{ij} = \frac{(i\tilde{\mu}|j\tilde{\nu})}{\epsilon_{\tilde{\mu}} + \epsilon_{\tilde{\nu}} - f_{ii} - f_{jj}}, \quad (44)$$

where  $f_{ii}$  and  $f_{jj}$  are occupied orbital energies, and  $\epsilon_{\tilde{\mu}}$  or  $\epsilon_{\tilde{\nu}}$  are PAO orbital energies obtained by diagonalization of the Fock matrix transformed to PAO space. The transformation matrices  $\mathbf{d}^{ij}$  transforming orbitals from PAO space to PNO space and occupation numbers  $n^{ij}$  correspond to eigenvectors and eigenvalues of the diagonalized matrix  $\mathbf{D}^{ij}$ :

$$\mathbf{D}^{ij} \mathbf{d}^{ij} = n^{ij} \mathbf{d}^{ij}. \quad (45)$$

The introduction of  $ij$ -specific PNO spaces, which are mutually non-orthogonal, leads to more complicated expressions in the amplitude equations because we also need to involve overlap matrices between different PNO spaces. The matrix transforming  $ij$ -PNO space to  $kl$ -PNO space  $S_{\tilde{a}_{ij}\tilde{b}_{kl}}^{ij;kl}$  is defined as

$$S^{ij;kl} = \mathbf{d}^{ij\dagger} \mathbf{S}^{\text{PAO}} \mathbf{d}^{kl}, \quad (46)$$

where  $\mathbf{S}^{\text{PAO}}$  is PAO overlap matrix. Thus, when considering the PNO space, the term in Eq. 21 can take the form

$$\frac{1}{4} v_{mn}^{\tilde{e}_{ij}\tilde{f}_{ij}} t_{\tilde{e}_{ij}\tilde{f}_{ij}}^{ij} t_{\tilde{a}_{mn}\tilde{b}_{mn}}^{mn} S_{\tilde{a}_{mn}\tilde{a}_{ij}}^{mn;ij} S_{\tilde{b}_{mn}\tilde{b}_{ij}}^{mn;ij} S_{\tilde{e}_{mn}\tilde{e}_{ij}}^{mn;ij} S_{\tilde{f}_{mn}\tilde{f}_{ij}}^{mn;ij}. \quad (47)$$

However, it is also possible to transform  $e, f$  indices from  $ij$ - to  $mn$ -PNO space first and then to perform the contraction of the integral with the first amplitude. The complex structure of these terms significantly expands the possibilities of how the terms can be factorized. The cost is also affected by the integral evaluation, which depends on the available memory.

We can pre-compute not only  $v_{ij}^{\tilde{e}_{ij}\tilde{f}_{ij}}$  type of integrals, but also some mixed PNO space integrals (only those which will be needed).

In our work, we assume that we will utilize a larger number of nodes, so we will have more memory and computing effort available. In that case, we can afford tighter thresholds, leading to larger domains and PNO spaces, which means higher precision in the recovery of the correlation energy. For the implementation of DLPNO formulations in TAMM, we employed a code generator implemented in Python that transforms the canonical equations by the transformation rules for various spaces (i.e., PNO, PAO, etc.). Using a code generator allowed us to systematically convert equations while automatically applying an operation cost minimization algorithm for single-term optimization. We anticipate that these kinds of code generators on the high-level equations enable trying different transformations and automatically choosing the best performing one. While this implementation is in the early stages, we were able to validate the correctness of generated code using our infrastructure to directly compare the results with canonical counterparts.

The perturbative correction (T) described in Sec. 4.1.2 is in the local version evaluated using the same equations with some differences.<sup>85</sup> While converged  $T_1$  and  $T_2$  amplitudes

are obtained in their PNO space, the virtual indices in terms  $A_{ijk}^{abc}$  or  $B_{ijk}^{abc}$  are represented in triples natural orbitals (TNO), which are computed from triplet density matrix obtained from three pair density matrices  $\mathbf{D}^{ijk} = 1/3(\mathbf{D}^{ij} + \mathbf{D}^{ik} + \mathbf{D}^{jk})$ . In order to perform contractions of integrals and amplitudes in Eqs. 27 and 29, we need to involve transformation matrices between PNO and TNO spaces  $\mathbf{S}^{ij:klm}$ , which are computed the same way as in Eq. 46 where  $\mathbf{d}^{kl}$  is replaced by  $\mathbf{d}^{klm}$ , transforming PAO orbitals to TNO space. Similar to DLPNO CCSD implementation, we leveraged the TAMM framework’s dense tensor infrastructure to represent the perturbation correction implementation with block-sparse computation. Using the PNO representation of the amplitudes from CCSD implementation, we implemented the DLPNO formulation of the canonical equations.

#### D. Time-dependent Coupled-Cluster Method

In addition to the stationary and frequency-dependent formulations of CC theory, one could witness significant progress on our end in developing a time-dependent CC method for simulating real-time dynamics.

The TDCC method has been studied in the context of the CC linear-response theory,<sup>63,64,86–88</sup> X-ray spectroscopy and Green’s function theory,<sup>89–93</sup> nuclear physics,<sup>94–96</sup> condensed matter physics,<sup>70</sup> and quantum dynamics of molecular systems in external fields.<sup>97–102</sup> These studies have also initiated an intensive effort towards understanding many aspects of the TDCC formalism, including addressing fundamental problems such as the form of the action functional, the form of the time-dependent molecular orbital basis, physical interpretation of time-dependent orbitals, various-rank approximations of the cluster operator, and numerical stability of time integration algorithms. One of the milestone achievements in developing time-dependent CC formalism was Arponen’s action functional for the bi-variational coupled cluster formalism<sup>70</sup> and following analysis by Kvaal considering time-varying orbitals.<sup>98</sup>

The time-dependent Schrödinger equation (TDSE),

$$i\partial_\tau|\Psi(\tau)\rangle = H|\Psi(\tau)\rangle, \quad (48)$$

is an initial value problem, which has a formal solution  $|\Psi(\tau)\rangle = e^{-iH\tau}|\Psi\rangle$ , with the initial condition,  $|\Psi(0)\rangle = |\Psi\rangle$ . An efficient way of finding approximate solutions of the TDSE for many-electron systems is associated with the utilization of the time-dependent CC (TD-CC) Ansatz

$$|\Psi(\tau)\rangle = e^{T(\tau)}|\Phi\rangle. \quad (49)$$

Upon plugging TD-CC Ansatz into the Eqn 48, and projecting onto the excited determinants, one obtains

$$i\partial_\tau\langle\Phi_{i_1\dots i_k}^{a_1\dots a_k}|T(\tau)|\Phi\rangle = \langle\Phi_{i_1\dots i_k}^{a_1\dots a_k}|\bar{H}(\tau)|\Phi\rangle \quad (50)$$

where  $T(\tau)$  is time-dependent cluster operator,  $|\Phi\rangle$  is a time-independent reference wave function in our consideration, and  $\bar{H}(\tau) = e^{-T(\tau)}He^{T(\tau)}$ , is the similarity transformed time-dependent Hamiltonian, which is the generator for the time evolution.

The similarity transformed CC Hamiltonian is non-Hermitian. Therefore, the computation of observables in this framework requires a bi-variational approach,<sup>60,70</sup> i.e., both the bra and ket states must be varied independently. The expectation value of any observable in TDCC framework is defined as,

$$\langle O \rangle = \langle \Phi | (1 + \Lambda(\tau)) \bar{O}(\tau) | \Phi \rangle \quad (51)$$

where  $\Lambda$  is a de-excitation operator. For obtaining equations for the  $\Lambda$ , we write down the TDSE,  $-i\partial_\tau\langle\Psi'(\tau)| = \langle\Psi'(\tau)|H$ , for the bra vector, with  $H = H^\dagger$ ,

$$-i\partial_\tau\langle\Phi|(1 + \Lambda(\tau))e^{-T(\tau)} = \langle\Phi|(1 + \Lambda(\tau))e^{-T(\tau)}H \quad (52)$$

Multiplying by  $e^{T(\tau)}$  from the right, and right projecting to the excited determinants obtains

$$-i\partial_\tau\langle\Phi|\Lambda(\tau)|\Phi_{a_1\dots a_k}^{i_1\dots i_k}\rangle = \langle\Phi|(1 + \Lambda(\tau))\bar{H}(\tau)|\Phi_{a_1\dots a_k}^{i_1\dots i_k}\rangle \quad (53)$$

The TAMM infrastructure has been utilized to implement the time evolution of the  $T(\tau)$  operator. We have considered singles (S) and doubles (D) excitation approximations in our implementation. Our implementation uses Cholesky-decomposed two-body electron repulsion matrix elements,<sup>103,104</sup> and we exploit spin-explicit formalism to evaluate tensor contractions of matrix elements of various operators.

#### V. CONCLUSION

In this paper, we present the Tensor Algebra for Many-body Methods framework that enables scalable and performance-portable implementations of important computational chemistry methods on large-scale heterogeneous high-performance computing systems. We described the TAMM framework in detail by introducing a tensor algebra interface that leverages high-level representation of the tensor algebra operations as an embedded domain-specific language. This interface enables separation of concerns between scientific application development and high-performance computing development efforts. The domain scientist or scientific application developer can focus on the method development instead of the performance optimization details, whereas the HPC developers focus on the underlying algorithms and optimizations. Later, we presented our modular infrastructure that allows the implementation of different optimizations on tensor data distribution, execution, and scheduling of tensor operations for efficient execution on modern heterogeneous HPC platforms. Finally, we showcased the performance and productivity benefits of using the TAMM framework for implementing complete computational chemistry applications that can be expressed as operations on tensors through various case studies.

#### ACKNOWLEDGMENTS

This research was supported by the Exascale Computing Project (17-SC-20-SC), a collaborative effort of the U.S. Department of Energy Office of Science and the National Nuclear

Security Administration, and by the Center for Scalable Predictive Methods for Excitations and Correlated Phenomena (SPEC), which is funded by the U.S. Department of Energy (DoE), Office of Science, Office of Basic Energy Sciences, Division of Chemical Sciences, Geosciences and Biosciences as part of the Computational Chemical Sciences (CCS) program at Pacific Northwest National Laboratory (PNNL) under FWP 70942. PNNL is a multi-program national laboratory operated by Battelle Memorial Institute for the U.S. DoE under Contract DE-AC06-76RLO-1830. NPB also acknowledges support from the Laboratory Directed Research and Development (LDRD) Program at PNNL. This research used resources of the Oak Ridge Leadership Computing Facility, which is a DOE Office of Science User Facility supported under Contract DE-AC05-00OR22725.

## VI. AUTHOR DECLARATIONS

### A. Conflict of Interest

The authors have no conflict of interest to declare.

## VII. DATA AVAILABILITY

The data that support the findings of this study are available from the corresponding author upon reasonable request.

## REFERENCES

- <sup>1</sup>N. G. A. B. Ajay Panyala, Erdal Mutlu and S. Krishnamoorthy, TAMM: Tensor algebra for many-body methods, <https://github.com/NWChemEx-Project/TAMM>, 2022.
- <sup>2</sup>F. Coester, Nucl. Phys. **7**, 421 (1958).
- <sup>3</sup>F. Coester and H. Kummel, Nucl. Phys. **17**, 477 (1960).
- <sup>4</sup>J. Čížek, J. Chem. Phys. **45**, 4256 (1966).
- <sup>5</sup>G. D. Purvis and R. J. Bartlett, J. Chem. Phys. **76**, 1910 (1982).
- <sup>6</sup>J. Paldus, J. Čížek, and I. Shavitt, Phys. Rev. A **5**, 50 (1972).
- <sup>7</sup>J. Paldus and X. Li, Adv. Chem. Phys. **110**, 1 (1999).
- <sup>8</sup>T. D. Crawford and H. F. Schaefer, Rev. Comput. Chem. **14**, 33 (2000).
- <sup>9</sup>R. J. Bartlett and M. Musiał, Rev. Mod. Phys. **79**, 291 (2007).
- <sup>10</sup>K. Raghavachari, G. Trucks, J. A. Pople, and M. Head-Gordon, Chem. Phys. Lett. **157**, 479 (1989).
- <sup>11</sup>C. Hampel and H.-J. Werner, J. Chem. Phys. **104**, 6286 (1996).
- <sup>12</sup>M. Schütz, J. Chem. Phys. **113**, 9986 (2000).
- <sup>13</sup>M. Schütz and H.-J. Werner, Chem. Phys. Lett. **318**, 370 (2000).
- <sup>14</sup>F. Neese, F. Wennmohs, and A. Hansen, J. Chem. Phys. **130**, 114108 (2009).
- <sup>15</sup>C. Riplinger and F. Neese, J. Chem. Phys. **138**, 034106 (2013).
- <sup>16</sup>P. Pinski, C. Riplinger, E. F. Valeev, and F. Neese, J. Chem. Phys. **143**, 034108 (2015), <https://doi.org/10.1063/1.4926879>.
- <sup>17</sup>C. Riplinger, P. Pinski, U. Becker, E. F. Valeev, and F. Neese, J. Chem. Phys. **144**, 024109 (2016).
- <sup>18</sup>F. Pavosevic, P. Pinski, C. Riplinger, F. Neese, and E. F. Valeev, J. Chem. Phys. **144** (2016).
- <sup>19</sup>M. Saitow, U. Becker, C. Riplinger, E. F. Valeev, and F. Neese, J. Chem. Phys. **146**, 164105 (2017).
- <sup>20</sup><https://nwchemex-project.github.io/NWChemEx/>.
- <sup>21</sup><https://spec.labworks.org/home>.
- <sup>22</sup>S. Hirata, J. Phys. Chem A **107**, 9887 (2003).
- <sup>23</sup>M. Valiev *et al.*, Comput. Phys. Commun. **181**, 1477 (2010).
- <sup>24</sup>G. Baumgartner *et al.*, Proceedings of the IEEE **93**, 276 (2005).
- <sup>25</sup>J. A. Gunnels, F. G. Gustavson, G. M. Henry, and R. A. van de Geijn, ACM Trans. Math. Softw. **27**, 422 (2001).
- <sup>26</sup>M. Schatz, R. van de Geijn, and J. Poulson, SIAM Journal on Scientific Computing **38**, C748 (2016).
- <sup>27</sup>M. D. Schatz, T. M. Low, R. A. van de Geijn, and T. G. Kolda, SIAM J. Scientific Computing **36** (2014).
- <sup>28</sup>J. Poulson, B. Marker, R. A. van de Geijn, J. R. Hammond, and N. A. Romero, ACM Trans. Math. Softw. **39**, 13:1 (2013).
- <sup>29</sup>E. Solomonik, D. Matthews, J. R. Hammond, J. F. Stanton, and J. Demmel, Journal of Parallel and Distributed Computing **74**, 3176 (2014), Domain-Specific Languages and High-Level Frameworks for High-Performance Computing.
- <sup>30</sup>E. Epifanovsky *et al.*, J. Comput. Chem. **34**, 2293 (2013), <https://onlinelibrary.wiley.com/doi/pdf/10.1002/jcc.23377>.
- <sup>31</sup>K. Z. Ibrahim, S. W. Williams, E. Epifanovsky, and A. I. Krylov, Analysis and tuning of libtensor framework on multicore architectures, in *2014 21st International Conference on High Performance Computing (HiPC)*, pp. 1–10, 2014.
- <sup>32</sup>E. Solomonik and T. Hoefler, arXiv e-prints, arXiv:1512.00066 (2015), 1512.00066.
- <sup>33</sup>S. Manzer, E. Epifanovsky, A. I. Krylov, and M. Head-Gordon, J. Chem. Theory Comput. **13**, 1108 (2017).
- <sup>34</sup>F. Neese, F. Wennmohs, U. Becker, and C. Riplinger, J. Chem. Phys. **152**, 224108 (2020).
- <sup>35</sup>J. A. Calvin and E. F. Valeev, TiledArray: A general-purpose scalable block-sparse tensor framework, <https://github.com/valeevgroup/tiledarray>, 2019.
- <sup>36</sup>C. Peng, J. A. Calvin, F. Pavošević, J. Zhang, and E. F. Valeev, J. Phys. Chem A **120**, 10231 (2016).
- <sup>37</sup>R. Harrison *et al.*, SIAM Journal on Scientific Computing **38**, S123 (2016), <https://doi.org/10.1137/15M1026171>.
- <sup>38</sup>D. I. Lyakh, International Journal of Quantum Chemistry **119**, e25926 (2019), <https://onlinelibrary.wiley.com/doi/pdf/10.1002/qua.25926>.
- <sup>39</sup>P. Springer, T. Su, and P. Bientinesi, p. 56 (2017).
- <sup>40</sup>V. Anisimov, LibreTT - tensor transpose library., <https://github.com/victor-anisimov/Librett>, 2021.
- <sup>41</sup>J. Nieplocha *et al.*, The International Journal of High Performance Computing Applications **20**, 203 (2006).
- <sup>42</sup>E. Mutlu, K. Kowalski, and S. Krishnamoorthy, Toward generalized tensor algebra for ab initio quantum chemistry methods, in *Proceedings of the 6th ACM SIGPLAN International Workshop on Libraries, Languages and Compilers for Array Programming*, pp. 46–56, 2019.
- <sup>43</sup>R. A. Van De Geijn and J. Watts, Concurrency: Practice and Experience **9**, 255 (1997), <https://onlinelibrary.wiley.com/doi/pdf/10.1002/>
- <sup>44</sup>F. G. Van Zee and R. A. van de Geijn, ACM Trans. Math. Softw. **41** (2015).
- <sup>45</sup>J. Kim *et al.*, A code generator for high-performance tensor contractions on gpus, in *IEEE/ACM International Symposium on Code Generation and Optimization, CGO 2019, Washington, DC, USA, February 16-20, 2019*, pp. 85–95, IEEE, 2019.
- <sup>46</sup>K. K. A. P. E. M. N. G. J. K. A. B. Bo Peng, Nicholas Bauman and S. Krishnamoorthy, Nwchemex coupled cluster, <https://github.com/NWChemEx-Project/CoupledCluster>, 2022.
- <sup>47</sup>K. Kowalski, S. Krishnamoorthy, R. M. Olson, V. Tipparaju, and E. Apra, Scalable implementations of accurate excited-state coupled cluster theories: Application of high-level methods to porphyrin-based systems, in *Proceedings of 2011 International Conference for High Performance Computing, Networking, Storage and Analysis*, pp. 1–10, 2011.
- <sup>48</sup>H.-S. Hu, K. Bhaskaran-Nair, E. Apra, N. Govind, and K. Kowalski, J. Phys. Chem A **118**, 9087 (2014).
- <sup>49</sup>M. Rätsep, Z.-L. Cai, J. R. Reimers, and A. Freiberg, J. Chem. Phys. **134**, 01B608 (2011).
- <sup>50</sup>A. F. Collings and C. Critchley, *Artificial photosynthesis: from basic biology to industrial application* (John Wiley & Sons, 2007).
- <sup>51</sup>M. B. Smith and J. Michl, Chem. Rev. **110**, 6891 (2010).
- <sup>52</sup>C. Wang, D. E. Schlaminginger, V. Desai, and M. J. Tauber, ChemPhysChem **12**, 2891 (2011).
- <sup>53</sup>C. Wang, C. J. Berg, C.-C. Hsu, B. A. Merrill, and M. J. Tauber, J. Phys. Chem. B **116**, 10617 (2012).
- <sup>54</sup>O. R. L. C. Facility, Oak ridge leadership computing facility, 2020.

- <sup>55</sup>E. Apra *et al.*, J. Chem. Phys. **152**, 184102 (2020).
- <sup>56</sup>J. F. Stanton, Chem. Phys. Lett. **281**, 130 (1997).
- <sup>57</sup>J. Kim *et al.*, Scalable heterogeneous execution of a coupled-cluster model with perturbative triples, in *SC20: International Conference for High Performance Computing, Networking, Storage and Analysis*, pp. 1–15, 2020.
- <sup>58</sup>J. Geertsen, M. Rittby, and R. J. Bartlett, Chem. Phys. Lett. **164**, 57 (1989).
- <sup>59</sup>D. C. Comeau and R. J. Bartlett, Chem. Phys. Lett. **207**, 414 (1993).
- <sup>60</sup>J. F. Stanton and R. J. Bartlett, J. Chem. Phys. **98**, 7029 (1993).
- <sup>61</sup>P. Piecuch and R. J. Bartlett, *EOMXCC: A New Coupled-Cluster Method for Electronic Excited States*, Advances in Quantum Chemistry Vol. 34 (Academic Press, 1999), pp. 295–380.
- <sup>62</sup>K. Kowalski and P. Piecuch, J. Chem. Phys. **115**, 643 (2001).
- <sup>63</sup>H. J. Monkhorst, Int. J. Quantum Chem. **12**, 421 (1977).
- <sup>64</sup>H. Koch and P. Jørgensen, J. Chem. Phys. **93**, 3333 (1990).
- <sup>65</sup>H. Koch, O. Christiansen, P. Jørgensen, A. M. S. de Merás, and T. Helgaker, J. Chem. Phys. **106**, 1808 (1997).
- <sup>66</sup>M. Nooijen and J. G. Snijders, Int. J. Quantum Chem. **44**, 55 (1992).
- <sup>67</sup>M. Nooijen and J. G. Snijders, Int. J. Quantum Chem. **48**, 15 (1993).
- <sup>68</sup>M. Nooijen and J. Snijders, J. Chem. Phys. **102**, 1681 (1995).
- <sup>69</sup>L. Meissner and R. Bartlett, Int. J. Quantum Chem. **48**, 67 (1993).
- <sup>70</sup>J. Arponen, Ann. Phys. **151**, 311 (1983).
- <sup>71</sup>K. Bhaskaran-Nair, K. Kowalski, and W. A. Shelton, J. Chem. Phys. **144**, 144101 (2016).
- <sup>72</sup>B. Peng and K. Kowalski, Mol. Phys. **116**, 561 (2018).
- <sup>73</sup>A. P. Bo Peng, Karol Kowalski and S. Krishnamoorthy, GFCCLib: Green’s function coupled cluster library, <https://github.com/spec-org/gfcc>, 2020.
- <sup>74</sup>B. Peng, A. Panyala, K. Kowalski, and S. Krishnamoorthy, Comput. Phys. Commun. **265**, 108000 (2021).
- <sup>75</sup>A. Altun, M. Garcia-Ratés, F. Neese, and G. Bistoni, **12**, 12785 (2021).
- <sup>76</sup>J. M. Foster and S. F. Boys, Rev. Mod. Phys. **32**, 300 (1960).
- <sup>77</sup>J. Pipek and P. G. Mezey, J. Chem. Phys. **90**, 4916 (1989).
- <sup>78</sup>C. Hampel and H.-J. Werner, J. Chem. Phys. **104**, 6286 (1996).
- <sup>79</sup>M. Schütz and H.-J. Werner, J. Chem. Phys. **114**, 661 (2001).
- <sup>80</sup>M. Schutz, Phys. Chem. Chem. Phys. **4**, 3941 (2002).
- <sup>81</sup>C. Edmiston and M. Krauss, J. Chem. Phys. **42**, 1119 (1965).
- <sup>82</sup>R. Ahlrichs and W. Kutzelnigg, Theor. Chim. Acta **10**, 377 (1968).
- <sup>83</sup>Y. Guo, K. Sivalingam, E. F. Valeev, and F. Neese, J. Chem. Phys. **144**, 094111 (2016).
- <sup>84</sup>M. Schwilk, Q. Ma, C. Köppl, and H.-J. Werner, J. Chem. Theory Comput. **13**, 3650 (2017).
- <sup>85</sup>C. Riplinger, B. Sandhoefer, A. Hansen, and F. Neese, J. Chem. Phys. **139**, 134101 (2013).
- <sup>86</sup>D. Mukherjee and P. Mukherjee, Chem. Phys. **39**, 325 (1979).
- <sup>87</sup>E. Dalgaard and H. J. Monkhorst, Phys. Rev. A **28**, 1217 (1983).
- <sup>88</sup>H. Koch and P. Jørgensen, J. Chem. Phys. **93**, 3333 (1990).
- <sup>89</sup>K. Schönhammer and O. Gunnarsson, Phys. Rev. B **18**, 6606 (1978).
- <sup>90</sup>D. R. Nascimento and A. E. DePrince III, J. Phys. Chem. Lett. **8**, 2951 (2017).
- <sup>91</sup>J. J. Rehr *et al.*, J. Chem. Phys. **152**, 174113 (2020).
- <sup>92</sup>F. D. Vila, J. J. Kas, J. J. Rehr, K. Kowalski, and B. Peng, Front. Chem. **9**, 734945 (2021).
- <sup>93</sup>F. Vila, K. Kowalski, B. Peng, J. Kas, and J. Rehr, J. Chem. Theory Comput. **18**, 1799 (2022).
- <sup>94</sup>P. Hoodbhoy and J. W. Negele, Phys. Rev. C **18**, 2380 (1978).
- <sup>95</sup>P. Hoodbhoy and J. W. Negele, Phys. Rev. C **19**, 1971 (1979).
- <sup>96</sup>D. A. Pigg, G. Hagen, H. Nam, and T. Papenbrock, Phys. Rev. C **86**, 014308 (2012).
- <sup>97</sup>C. Huber and T. Klamroth, J. Chem. Phys. **134**, 054113 (2011).
- <sup>98</sup>S. Kvaal, J. Chem. Phys. **136**, 194109 (2012).
- <sup>99</sup>T. B. Pedersen and S. Kvaal, J. Chem. Phys. **150**, 144106 (2019).
- <sup>100</sup>H. E. Kristiansen, Ø. S. Schøyen, S. Kvaal, and T. B. Pedersen, J. Chem. Phys. **152**, 071102 (2020).
- <sup>101</sup>T. Sato, H. Pathak, Y. Orimo, and K. L. Ishikawa, J. Chem. Phys. **148**, 051101 (2018).
- <sup>102</sup>H. Pathak, T. Sato, and K. L. Ishikawa, J. Chem. Phys. **152**, 124115 (2020).
- <sup>103</sup>B. Peng and K. Kowalski, Chem. Phys. Lett. **672**, 47 (2017).
- <sup>104</sup>B. Peng and K. Kowalski, J. Chem. Theory Comput. **13**, 4179 (2017).